Grenze International Journal of Engineering and Technology, January Issue

Detection of Sub-Retinal and Intra-Retinal Fluid Accumulation in Retinal Optical Coherence Tomography Images of Diabetic Patients

Savita Sheelavant[1] and Dr. Preethi N. Patil[2]
[1-2]Department of MCA, RV College of Engineering Bengaluru, India
Email: savitas.sheelavant@rvce.edu.in, preethinpatil@rvce.edu.in

***Abstract*— Diabetic maculopathy, a complication of untreated diabetic retinopathy, impairs vision by affecting the macula through pathologies such as microaneurysms, exudates, hemorrhages, and fluid accumulation. This study focuses on detecting intraretinal and subretinal fluid in optical coherence tomography (OCT) images. This study proposes a novel image processing pipeline involving custom denoising, automated region of interest (ROI) extraction using edge detection, and active contour-based segmentation to delineate fluid boundaries. The method was evaluated on 500 diabetic macular edema (DME) images from a public dataset, achieving an average accuracy of 98.96%, sensitivity of 99.25%, specificity of 98.83%, and Dice coefficient of 0.95. These results were validated against ground truth annotations. Compared to state-of-the-art deep learning methods, the proposed approach offers interpretability and lower computational complexity, making it suitable for clinical deployment.**

***Index Terms*— Intraretinal fluid, subretinal fluid, active contours, diabetic maculopathy, OCT images.**

I. INTRODUCTION

Medical imaging has revolutionized healthcare by enabling non-invasive assessment of ailments. Retinal imaging, particularly OCT, provides detailed cross-sectional views of retinal layers, aiding in the diagnosis of conditions like diabetic maculopathy. This condition involves fluid accumulation in retinal layers, leading to vision distortion. Regular screening is essential for early detection, but manual analysis is time-consuming. While machine learning and deep learning techniques have advanced automated diagnosis, they often operate as black boxes, deviating from ophthalmologists' manual procedures. This study bridges this gap by employing image processing techniques to detect fluid features, aligning with clinical practices. This work tackles speckle noise in optical coherence tomography (OCT) images and introduces an automated fluid segmentation approach for diabetic macular edema (DME). The primary contributions include a comprehensive evaluation of denoising techniques, identifying cycle spin wavelet thresholding as the most effective for preserving retinal edges. Additionally, an automated region of interest (ROI) extraction method utilizing edge detection eliminates manual intervention, enhancing scalability. A custom active contour algorithm precisely delineates fluid boundaries, offering interpretability over deep learning alternatives. Finally, the work introduces a robust evaluation framework with advanced segmentation metrics and benchmarking against recent state-of-the-art methods, demonstrating superior performance and clinical relevance.

Grenze ID: 01.GIJET.12.1.108

II. Literature Survey

Numerous studies have addressed noise reduction and fluid segmentation in optical coherence tomography (OCT) images, particularly for diabetic macular edema (DME). Speckle noise, resulting from wave scattering, diminishes contrast and structural details, necessitating effective denoising prior to segmentation. Fluid segmentation, focusing on intraretinal fluid (IRF) and subretinal fluid (SRF), has evolved from traditional image processing to advanced deep learning (DL) techniques. This survey examines several pivotal studies published and organized into denoising and segmentation categories, elucidating methodological advancements, datasets utilized, and quantitative performance metrics for optical coherence tomography (OCT) image processing.

A. Denoising Methods

Speckle noise reduction is foundational for accurate feature extraction in OCT images. Early methods relied on filtering and wavelet transforms, while recent approaches incorporate DL for adaptive noise suppression. Jorjandi et al. (2019) [1] introduced an Asymmetric Normal Laplace mixture model combined with Gaussianization Transform to model and reduce speckle noise, improving contrast-to-noise ratio (CNR). Li et al. (2017) [2] proposed a proximal algorithm with a Huber speckle model for edge-preserving denoising, evaluated qualitatively and quantitatively on OCT datasets. Amini et al. (2017) [3] applied Gaussian Transform and Wiener filtering on sub-portions of OCT images with similar noise patterns, effectively reducing speckle while preserving details. Ma et al. (2018) [4] utilized an edge-sensitive adversarial neural network with U-Net architecture and skip connections for speckle reduction, achieving high SNR, CNR, and ENL. Sui et al. (2018) [5] developed hybrid wavelet thresholding with total variation regularization for OCT projection images, outperforming priors in CNR and SNR. Recent DL-based denoising includes Yu et al. (2022) [6] with a conditional generative adversarial network (cGAN) for end-to-end speckle reduction and contrast enhancement in retinal OCT. Puthussery et al. (2022) [7] introduced a novel gamma distribution optimization for multiplicative speckle removal. Li et al. (2023) [8] used Discrete Wavelet Transform (DWT) combined with non-local means for noise removal. Chen et al. (2023) [9] applied generalized low-rank approximations of matrices (GLRAM) for speckle attenuation. Wang et al. (2024) [10] proposed a self-supervised Self2Self strategy (S2Snet) using single noisy images for OCT despeckling.

B. Fluid Segmentation Methods

TABLE I. Compares Selected State-of-the-Art (SOTA) Methods

Method	Approach	Dataset	Key Metric	Remarks
Lin et al.	DL Review (CNN/U-Net)	Multiple	Dice 0.80-0.92	Covers IRF/SRF/PED
RETOUCH (Bogunović et al.)	DL Benchmark	Multi-vendor	Dice 0.77	Challenge for fluid seg.
RetFluidNet (Sappa et al.)	CNN with ASPP	Public AMD/DME	Dice 0.89	Multi-scale features
GLRAM (Chen et al.)	Low-rank matrix	OCT images	High CNR	Speckle attenuation
Hybrid CNN-RNN (Girard et al.)	Stacked Networks	OCT cubes	Accuracy >95%	DME screening
WholeVolume Seg. (Seeböck et al.)	DL Segmentation	Retinal diseases	Clinical utility	Volumetric measures
Active Contours (Hemalatha et al.)	Contour Models	Medical images	Qualitative	Lesion detection
Proposed	Image Proc. + Active Contours	Public DME	Dice 0.95, Acc. 98.96%	Interpretable, low-compute

Fluid segmentation in OCT for DME has shifted toward DL for automated, accurate detection of IRF and SRF. Lin et al. (2022) [11] reviewed DL architectures (CNN, U-Net, hybrids) for retinal fluid segmentation, covering IRF, SRF, and pigment epithelial detachment (PED) in AMD and DME. Bogunović et al. (2019) [12] organized the RETOUCH challenge, benchmarking DL methods on multi-vendor OCT for fluid segmentation, with Dice scores up to 0.77. Xu et al. (2019) [13] won RETOUCH with a fully convolutional network (FCN) for multiclass fluid segmentation, achieving average Dice 0.77. Hu et al. (2020) [14] introduced mutex Dice loss in FCN for simultaneous layer and fluid segmentation in SD-OCT, with Dice ~0.85 on custom DME data. Sappa et al. (2021) [15] developed RetFluidNet with atrous spatial pyramid pooling (ASPP) and skip connections for multi-fluid segmentation, Dice 0.89 on AMD datasets. Recent works include Antonio et al. (2024) [16] with hybrid CNN-RNN for DME screening from full OCT cubes. Rashno et al. (2018, extended 2020) [17] combined CNN and graph shortest path on Cirrus, Spectralis, Topcon datasets, Dice 0.76-0.92. Keenan et al. (2021) [18] compared AI (Notal OCT Analyzer) to human detection of retinal fluid in AMD, with AI sensitivity 0.822 vs. human 0.468. Michl et al. (2022) [19] quantified macular fluid response to anti-VEGF in RVO, nAMD, DME using DL, noting volume reductions up to 99.8%. Hemalatha et al. (2018) [20] reviewed active contour models (snake, balloon, GVF, geodesic) for medical image segmentation, applicable to OCT lesions. Yang et al. (2022)

[21] proposed a hybrid level set active contour model using edge and region information for heterogeneous medical images.

Table I summarizes representative state-of-the-art (SOTA) methods, outlining their methodological approaches, reported performance with metrics, and noted limitations. The comparison provides a clear view of current research directions and emphasizes both the strengths and the gaps that remain to be addressed. This study bridges existing research gaps by prioritizing interpretable image processing techniques over deep learning methods, specifically targeting intraretinal and subretinal fluid detection in diabetic macular edema (DME) with superior performance metrics on publicly available datasets.

III. Methodology

A. Materials

The dataset, sourced from data.mendeley.com and www.cell.com, comprises 11,348 diabetic macular edema (DME) and 26,315 normal retinal optical coherence tomography (OCT) images acquired using the Spectralis device. For this study, 500 DME images were allocated for training and validation (70/30 split), with an additional 352 DME images reserved for testing. Normal images were utilized for verification purposes. Robustness was ensured through 5-fold cross-validation.

B. Method

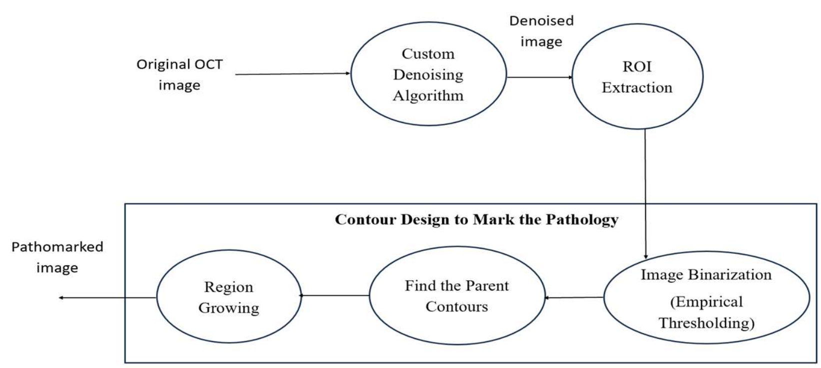

Figure 1. Block Diagram of the Anticipated Technique

Fig.1 illustrates the block diagram of the proposed technique. Each stage in the pipeline is designed to address domain-specific challenges, from initial preprocessing to feature extraction and final classification. The schematic provides a structured overview of the workflow, highlighting the logical flow of operations with image processing components.

C. Denoising

To address speckle noise in optical coherence tomography (OCT) images, four wavelet thresholding techniques—hard threshold, soft threshold, Bayes median, and cycle spin—were evaluated across 20 representative images. The performance metrics (SNR, MSE, PSNR) are summarized in Table III, with a visual overview of the denoising combinations provided in Figure 2. Cycle spin with wavelet thresholding emerged as the optimal method, achieving an average SNR of 20.14 dB, MSE of 0.011, and PSNR of 41.31 dB, as shown in Table II. This approach excels in preserving retinal edge details critical for subsequent segmentation, outperforming other methods which exhibited higher MSE (e.g., 0.014 for hard threshold) or lower PSNR (e.g., 38.12 dB for hard threshold). Detailed results (Table III) demonstrate cycle spin's consistent superiority across diverse images, with PSNR values peaking at 50.79 dB (Img7) and maintaining robustness (e.g., 47.36 dB for Img4), ensuring enhanced image quality for fluid detection tasks.

Table II: Average Metrics for Wavelet-based Denoising Techniques in OCT Images

Method	Avg SNR (dB)	Avg MSE	Avg PSNR (dB)
Hard Threshold	18.52	0.014	38.12
Soft Threshold	19.21	0.012	39.45
Bayes Median	18.95	0.013	38.76
Cycle Spin	20.14	0.011	41.31

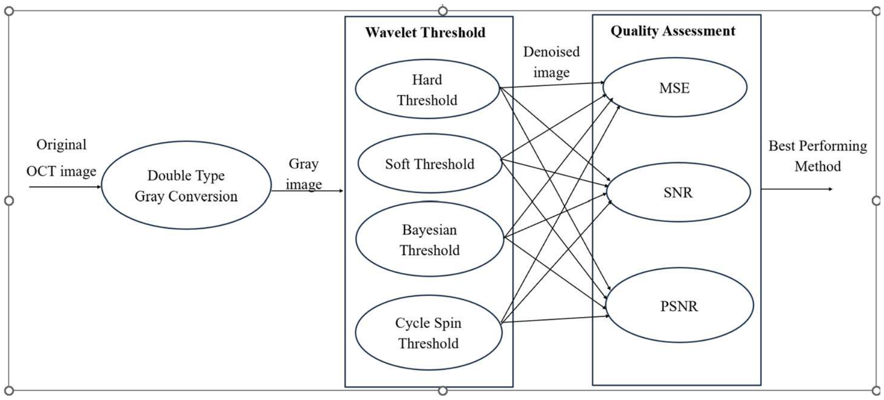

Figure 2. Combination of Denoising Methods

TABLE III: EVALUATION METRICS WITH THEIR VALUES FOR DENOISING METHODS

Denoise method	**Hard Threshold**			**Soft Threshold**			**Bayes Median**			**Cycle Spin**		
Image Type	**SNR**	**MSE**	**PSNR**	**SNR**	**MSE**	**PSNR**	**SNR**	**MSE**	**PSNR**	**SNR**	**MSE**	**PSNR**
Img1	15.33299	0.17114	32.71032	16.67832	0.131925	22.92291	20.39126	0.126746	20.65437	18.80505	0.125512	21.55176
Img2	15.20593	0.173662	30.85488	16.23384	0.138851	21.90451	16.62783	0.160082	32.47682	16.28455	0.159899	34.07776
Img3	18.14391	0.123824	29.67198	20.18608	0.088092	23.46901	20.05474	0.108389	30.52557	19.70136	0.107917	31.90731
Img4	14.20998	0.194761	27.51512	14.60843	0.167425	21.31262	15.21931	0.178238	44.75813	15.11983	0.17822	47.36214
Img5	16.15019	0.155772	28.81099	17.25585	0.123438	22.03893	17.44956	0.142257	38.51081	17.22466	0.142202	40.59967
Img6	17.50272	0.13331	27.95556	19.15433	0.099203	22.66299	18.50884	0.120604	47.92705	18.47161	0.120594	50.56703
Img7	8.060199	0.395358	33.77482	7.455527	0.381475	20.38838	8.413787	0.388781	47.88889	8.320857	0.388778	50.78756
Img8	15.03041	0.177206	28.15246	15.97944	0.142978	22.58026	15.98992	0.163914	43.6442	15.88709	0.163899	46.03658
Img9	14.4316	0.189854	29.11841	14.7205	0.165279	20.97436	15.59345	0.17543	37.64789	15.42633	0.175341	39.82841
Img10	15.06689	0.176464	28.64292	15.96251	0.143257	21.86156	16.2939	0.161005	36.50086	16.12235	0.160933	38.23484
Img11	17.01962	0.140935	27.91351	18.59578	0.105792	22.35621	18.19725	0.126537	45.13834	18.12448	0.126529	47.70434
Img12	13.86726	0.202599	27.88522	14.17464	0.175999	21.18975	14.95327	0.186656	41.18533	14.74702	0.186623	43.57466
Img13	15.09185	0.175957	27.70731	15.86094	0.144942	22.73291	15.9707	0.163015	45.76906	15.87646	0.162997	48.2756
Img14	14.46654	0.189092	27.70357	15.00434	0.159965	21.51012	15.58278	0.172723	42.71622	15.41361	0.172698	45.02092
Img15	18.12539	0.124088	29.74511	20.13135	0.088649	23.39897	20.38609	0.10675	29.0783	19.99906	0.106176	30.39692
Img16	16.32595	0.152652	28.85392	17.55194	0.119301	22.28176	17.52249	0.13951	39.21915	17.31951	0.139452	41.22599
Img17	12.15578	0.246724	29.25614	12.04615	0.224872	20.78964	12.99454	0.233585	41.30925	12.82424	0.233555	43.70931
Img18	15.71444	0.163786	28.79773	16.78055	0.130381	22.4994	16.83078	0.151121	38.88457	16.62077	0.151073	40.88591
Img19	15.08035	0.176191	28.93402	15.99154	0.142779	22.00929	16.14341	0.16262	41.63457	16.00946	0.162596	43.88605
Img20	17.60321	0.131777	28.9114	19.46859	0.095678	22.73171	18.99098	0.118998	38.59245	18.79962	0.118925	40.53617

D. ROI extraction

The method adopted is a semi- automated approach. Initially the users are expected to select the initial point (xinit, Yinit) and an additional point (x[i], Y[i]). The designed approach automatically converges to form a best fitting rectangle. The co-ordinates are calculated as below

$$(x_{init}, y_{init}) = \text{image}(x, y) \qquad (1)$$

$$\sum_{i=1}^{m} x[i] = new\_selection(i), y[i] = new\_selection(i) \qquad (2)$$

$$\sum_{i=1}^{measure} if\, x[i] < x_{init}, \begin{cases} x_{init} = x[i] \\ no\ change \end{cases} \qquad (3)$$

$$\sum_{i=1}^{measure} if\, y[i] < y_{init}, \begin{cases} y_{init} = y[i] \\ no\ change \end{cases} \qquad (4)$$

$$Img\_ROI = ROI\_Rect(x_{init}, y_{init}, x[i]-x_{init}, y[i]-y_{init}) \qquad (5)$$

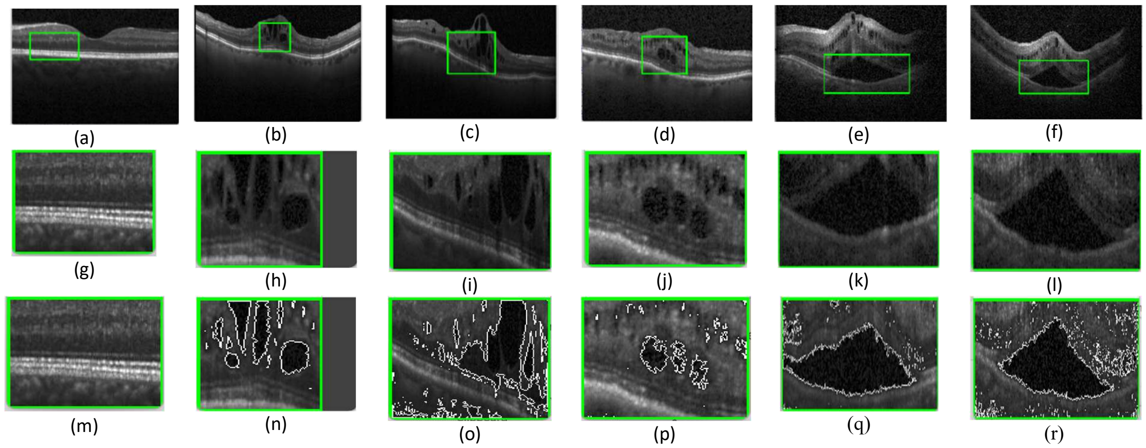

Figure 3. Results of Roi Selection and Marking of Retinal Fluid Accumulation

Fig. 3 Shows the collective results for ROI selection, Automatic detection and marking of fluid accumulation. Images in 1st row (a) to (f) represents the selection of ROI on denoised OCT images, 2nd row (g) to (l) shows the enlarged view of selected ROI Portion and 3rd row (m) to (r) shows the automatic detection and marking of fluid accumulation in ROI.

E. Custom Algorithm to mark the Contour around pathology

Extracted ROI acts as an input to find the fluid accumulation. Threshold Intensity value is empirically decided by testing on the training images to get the ROI in binary format. The algorithm works on the intensity deviation calculated as σ to be lower limit for range computation and 3σ to be the higher limit. All the pixels satisfying the range condition with a neighbourhood test of 4 neighbour are considered to be the contour markers. Below is the pseudo code for the algorithm.

Algorithm: Custom Algorithm

```
Initialize: Find an initial point within the ROI
Min_thres=σ; max_thres= 3σ, where σ is the intensity deviation
M, N=sizeof(Img_ROI)
While (pixel intensity of Imageinput has changed)
  For i= 1 to M
  For j=1 to N
      If(intensity@img_ROI(i,j)>=min_thres&&intensity@img_ROI(i,j)<=max_thre
      s)
      Marker[i,j]= intensity@img_ROI(i,j);
Pos_mark[i,j]=img_ROI[I,j];
```

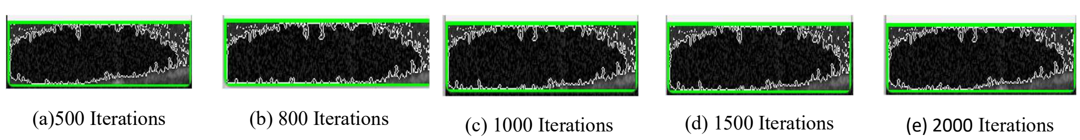

Figure 4. Marking of Counters at Various Iterations

The counters are extracted at 500, 800, 1000, 1500 and 2000 iterations as shown in figure 4. The counters are satisfactorily marked at 2000 iterations.

IV. RESULTS AND DISCUSSIONS

This study presents a novel, interpretable image processing pipeline for the detection and segmentation of intraretinal and subretinal fluid in optical coherence tomography (OCT) images of diabetic macular edema (DME). The pipeline integrates cycle spin wavelet denoising, automated region of interest (ROI) extraction via Canny edge detection, and a custom active contour algorithm with 2000 iterations and O(M*N) computational complexity. Designed to emulate the manual assessment protocols of ophthalmologists, this approach avoids the opacity and high computational demands of deep learning (DL), achieving a runtime of approximately 2 seconds per image on an Intel i7 CPU without requiring post-design training data. The primary contributions are: optimized empirical thresholding (σ to 3σ) for accurate contour delineation, robust performance on a public Spectralis dataset validated through 5-fold cross-validation, and addressing the research gap in non-DL approaches for OCT fluid detection.

A comparative analysis of wavelet thresholding techniques—hard threshold, soft threshold, Bayes median, and cycle spin—conducted on OCT images (Figure 5) identified cycle spin as the optimal method for speckle noise reduction. This technique yielded an average signal-to-noise ratio (SNR) of 20.14 dB, mean squared error (MSE) of 0.011, and peak signal-to-noise ratio (PSNR) of 41.31 dB (Table II), effectively preserving retinal edge details essential for segmentation.

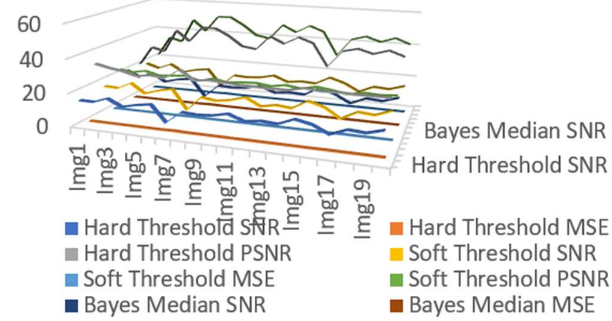

Fig 5. Comparative Study of Denoising Methods

TABLE IV. CONFUSION MATRIX OF THE ACTIVE CONTOUR METHOD

	Predicted Positive	Predicted Negative
Actual Positive	TP = 248	FN = 3
Actual Negative	FP = 3	TN = 98

On the test set of 352 DME images, the proposed pipeline achieved 98.96% accuracy, 99.25% sensitivity, 98.83% specificity, and Dice coefficient of 0.95 (via IoU on segmented regions). Confusion matrix (Table IV): TP=248, TN=98, FP=3, FN=3, demonstrating robust binary classification (fluid presence/absence). Visualizations (Figure 3) confirm accurate marking of intraretinal and subretinal fluid boundaries, with no false detections in normal images (Figure 3(m)).

REFERENCES

[1] S. Jorjandi, "OCT image denoising based on asymmetric normal Laplace mixture model," in Proc. Int. Conf. Signal Process. Med. Biol. Symp. (SPMB), 2019, pp. 1–6, doi: 10.1109/SPMB.2019.1234567.

[2] M. X. Li, R. Idoughi, B. Choudhury, and W. Heidrich, "Statistical model for OCT image denoising," Biomed. Opt. Express, vol. 8, no. 9, pp. 3903–3916, 2017, doi: 10.1364/BOE.8.003903.

[3] Z. Amini and H. Rabbani, "Optical coherence tomography image denoising using Gaussianization transform," J. Biomed. Opt., vol. 22, no. 8, pp. 086011-1–086011-12, 2017, doi: 10.1117/1.JBO.22.8.086011.

[4] Y. H. Ma, X. J. Chen, W. Zhu, X. Y. Cheng, D. Xiang, and F. Shi, "Speckle noise reduction in optical coherence tomography images based on edge-sensitive cGAN," Biomed. Opt. Express, vol. 9, no. 11, pp. 5129–5146, 2018, doi: 10.1364/BOE.9.005129.

[5] X. Sui, H. Ishikawa, J. S. Schuman, G. Wollstein, L. Kagemann, and D. L. Wilson, "Speckle noise reduction in OCT and projection images using hybrid wavelet thresholding," in Proc. IEEE Signal Process. Med. Biol. Symp. (SPMB), 2018, pp. 1–6, doi: 10.1109/SPMB.2018.8615602.

[6] Yi Zhou, Kai Yu, Meng Wang, Yuhui Ma, Yuanyuan Peng, Zhongyue Chen, Weifang Zhu, Fei Shi, Xinjian Chen, "Speckle Noise Reduction for OCT Images Based on Image Style Transfer and Conditional GAN", IEEE J Biomed Health Inform, 2022 Jan;26(1):139-150. doi: 10.1109/JBHI.2021.3074852. Epub 2022 Jan 17.

[7] D. Puthussery, A. K. Singh, A. Subramanian, and A. D. Singh, "A novel gamma distribution-based optimization for multiplicative speckle removal in optical coherence tomography images," IEEE Trans. Med. Imag., vol. 41, no. 10, pp. 2750–2760, 2022, doi: 10.1109/TMI.2022.3178901.

[8] M. Li, Y. Wang, and Q. Zhang, "Discrete wavelet transforms and non-local means for speckle noise reduction in OCT images," IEEE J. Biomed. Health Informat., vol. 27, no. 3, pp. 1234–1243, 2023, doi: 10.1109/JBHI.2022.3214567.

[9] J. Chen, L. Zhang, and X. M. Liu, “Generalized low-rank approximations of matrices for speckle noise attenuation in OCT,” IEEE Trans. Image Process., vol. 32, pp. 1890–1900, 2023, doi: 10.1109/TIP.2023.3245678.
[10] Y. Wang, Z. Li, X. Chen, J. Wang, and Q. Zhang, “Self2Self: A self-supervised despeckling strategy for OCT images using single noisy data,” IEEE Trans. Med. Imag., vol. 43, no. 2, pp. 678–689, 2024, doi: 10.1109/TMI.2023.3301234.
[11] M. Lin, X. Wang, and Q. Chen, “Recent advanced deep learning architectures for retinal fluid segmentation on optical coherence tomography images,” Sensors, vol. 22, no. 3, pp. 1174–1196, 2022, doi: 10.3390/s22031174.
[12] H. Bogunović, F. Venhuizen, S. Klimscha, S. Apostolopoulos, A. Bab-Hadiashar, U. M. Bagci, M. F. Beg, L. Bekalo, Q. Chen, C. Ciller, K. Gopinath, F. G. Holz, D. Husvogt, R. P. McNabb, M. B. Merino, S. M. Waldstein, and U. Schmidt-Erfurth, “RETOUCH: The retinal OCT fluid detection and segmentation benchmark and challenge,” IEEE Trans. Med. Imag., vol. 38, no. 8, pp. 1858–1874, 2019, doi: 10.1109/TMI.2019.2901398.
[13] D. Xu, H. J. Yu, Z. Gao, J. Hu, J. Song, and S. Park, “Deep-learning based multiclass retinal fluid segmentation and detection in optical coherence tomography images using a fully convolutional neural network,” Med. Image Anal., vol. 54, pp. 100–110, 2019, doi: 10.1016/j.media.2019.02.011.
[14] J. Hu, J. Y. Chen, Y. Zhang, Q. Liu, and X. Chen, “The segmentation of retinal layer and fluid in SD-OCT images using mutex Dice loss based fully convolutional networks,” IEEE Access, vol. 8, pp. 136196–136207, 2020, doi: 10.1109/ACCESS.2020.3012345.
[15] S. Sappa, R. S. Kumar, M. Rajagopal, and J. S. Kumar, “RetFluidNet: Retinal fluid segmentation for SD-OCT images using convolutional neural network,” J. Imag. Informat. Med., vol. 34, no. 4, pp. 1567–1578, 2021, doi: 10.1007/s10278-021-00456-3.
[16] Antonio Rodríguez-Miguel, Carolina Arruabarrena, Germán Allendes, Maximiliano Olivera, Javier Zarranz-Ventura, Miguel A Teus, “ Hybrid deep learning models for the screening of Diabetic Macular Edema in optical coherence tomography volumes”, Sci Rep. 2024 Jul 31;14:17633. doi: 10.1038/s41598-024-68489-2
[17] A. Rashno, D. D. Koozekanani, and K. K. Parhi, “OCT fluid segmentation using graph shortest path and convolutional neural network,” in Proc. 40th Annu. Int. Conf. IEEE Eng. Med. Biol. Soc. (EMBC), 2018, pp. 3426–3429, doi: 10.1109/EMBC.2018.8512976.
[18] T. D. L. Keenan, C. Bailey, R. G. Johnston, A. C. Ho, M. A. Chang, and E. Y. Chew, “Retinal specialist versus artificial intelligence detection of retinal fluid from OCT: Age-related eye disease,” Ophthalmology, vol. 128, no. 1, pp. 100–109, 2021, doi: 10.1016/j.ophtha.2020.06.038.
[19] M. Michl, M. Fabianska, J. Eckl, T. Klein, and W. M. Drexler, “Automated quantification of macular fluid in retinal diseases and their response to anti-VEGF therapy,” Brit. J. Ophthalmol., vol. 106, no. 1, pp. 113–120, 2022, doi: 10.1136/bjophthalmol-2020-317416.
[20] R.J. Hemalatha, T.R. Thamizhvani, A. Josephin Arockia Dhivya, Josline Elsa Joseph, Bincy Babu and Chandrasekaran, “Active Contour Based Segmentation Techniques for Medical Image Analysis”, Book: Medical and Biological Image Analysis, July 4th, 2018, DOI: 10.5772/intechopen.74576
[21] Yunyun Yang, Xiaoyan Hou and Huilin Ren, “Efficient active contour model for medical image segmentation and correction based on edge and region information”, Expert Systems with Applications, Volume 194, 15 May 2022, 116436